NUMERICAL MODELING AND SPECTROSCOPIC DIAGNOSTICS OF A PULSE-MODULATED INDUCTIVELY COUPLED PLASMA

R. Ye[1], H. Taguchi[1,2], H. Lange[3], N. Kobayashi[1,4], S. Ito[2], T. Watanabe[5] and T. Ishigaki[1]

[1] *Advanced Materials Laboratory, National Institute for Materials Science, 1-1 Namiki, Tsukuba, Ibaraki 305-0044, Japan*
[2] *Department of Pure and Applied Chemistry, Tokyo University of Science, Noda, Japan*
[3] *Department of Chemistry, Warsaw University, Poland*
[4] *Department of Nuclear Engineering, Tokyo Institute of Technology*
[5] *Department of Environmental Chemistry and Engineering Chemistry, Tokyo Institute of Technology*

Numerical modeling and spectroscopic diagnostics of an Ar-H_2 inductively coupled plasma under pulse-modulated power conditions were carried out. It was found that the predicted and measured electron number densities were in good agreement in the central region of the torch; while the observed discrepancies between them in the fringes of the plasma suggested the presence of departure form local thermodynamic equilibrium in those regions. The nonequilibrium effect became more appreciable in the plasma operated under the pulsed power conditions.

1. Introduction

Pulse-modulated inductively coupled plasmas (PM-ICPs) are characterized by their nonequilibrity and relatively high concentrations of chemically reactive radical species. Under pulsed power conditions, their enthalpies can be easily controlled by adjusting the high-low power ratio and the duty factor of pulsation, and their radiation losses can also be considerably reduced, compared with those of continuous plasmas [1-5]. These features are crucial to avoiding the overheating of specimen when processed in such environments with high heat fluxes. The PM-ICPs have shown some prominent advantages in materials processing, such as the doping of hydrogen into functional ceramics [6, 7].

In the past few years, a number of theoretical and experimental studies on induction plasmas operated under pulsed power conditions have been carried out [4, 8-10]. Most of those researches were concentrated on the dynamic behavior of PM-ICPs. The nonequilibrium phenomena in those plasmas were interpreted in terms of the temporal behavior of line emission intensities. However, work involving direct comparisons between experimentally and theoretically obtained results for pulsed power plasmas is likely lagging behind. In the present study, numerical modeling and spectroscopic diagnostics of an Ar-H_2 pulse-modulated inductively coupled plasma were carried out. The numerical modeling was performed using a renormalization group (RNG) *k-e* turbulence model with the local thermodynamic equilibrium (LTE) assumption [11]. The electron number densities were measured by using Stark broadening. Since the experimentally detected electron population densities were independent of the equilibrium conditions in the plasma, a comparison between the predicted LTE profiles of the plasma temperatures and the electron number densities and the measured ones should reveal more conceivable information on the nonequilibrium situations in such thermal plasma generators operated under pulsed power conditions.

2. Experimental set-up

The plasma torch and spectroscopic diagnostics systems for the present work are schematically shown in Figure 1. A voltage-control-type solid state amplifier (MP-22CY, Denki Kogyo Co., Ltd.) was used in the generation of pulsed power plasmas. An invert-type power source supplied an electric power of 22 kW continuously at a nominal frequency of 1 MHz. The power source and the load were electrically matched by using a phase-locked loop (PLL) with variable frequencies and an LC matching circuit. The radio frequency (RF) power was pulse-modulated by using an external pulsed signal generated by a pulse generator (HP-8116A)

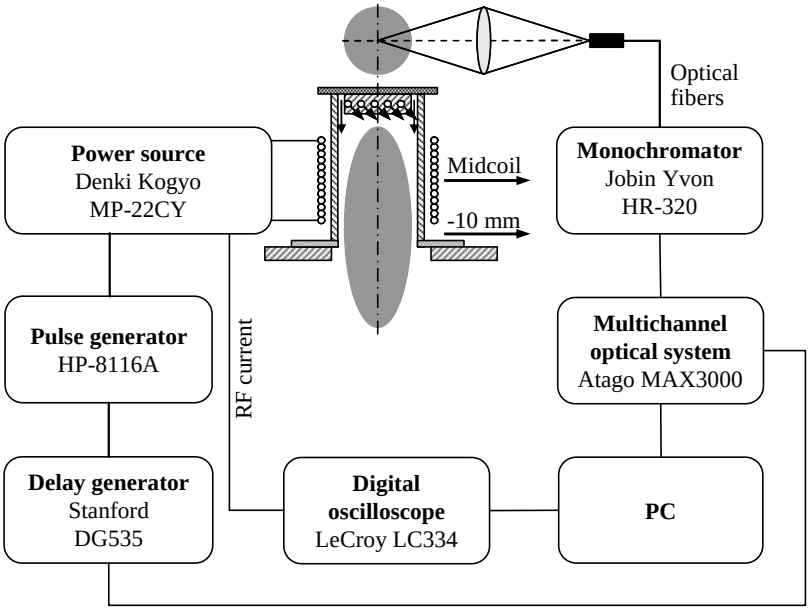

Figure 1. Schematic of the plasma generation and optical diagnostics systems.

to switch a static induction transistor in the power source. The rise time of the power source was less than 1 μs. The plasma was firstly generated at continuous power level of 13 kW and chamber pressure of 200 Torr. Then, the external pulse signal was imposed to switch the plate power from the continuous operating mode to the pulse-modulated one with pulse-on and pulse-off times of 10 and 5 ms, and high and low power levels of 13 and 4 kW, respectively.

The plasma line emissions were monitored at the middle of the RF coil and 10 mm below the last coil in the downstream direction. The optical systems for the measurements of the emission intensities were calibrated using a halogen lamp. The lights emitted from the plasma were focused by an optical system with a spatial resolution of 0.5 mm, and were transmitted to the monochromators through optical fibers. In order to obtain the radial profiles of the plasma emissions, the optical system was mounted on a displacement frame driven by a step motor. For the measurement of the electron temperature, the focused plasma radiations were monochromated using a JOBIN YVON HR-320, and the light signals for two hydrogen atomic lines (H_α: 656 nm and H_β: 486 nm) and were processed in a multichannel detection system (Atago MAX-3000). The time-resolved measurement was performed with a gate period of 10 μs, in which the delayed signal was given by a delay generator (Stanford DG535). The net emission intensities for the two spectral lines were obtained by subtracting the continuum component from the measured line intensities, and the temperature was then calculated using the two-line method. For the measurement of electron number density, the signal of the H_β line at 486 nm were processed. The coil current signals were stored in a PC through a digital oscilloscope (LeCroy LC334). The electron number density was determined using Stark broadening, and the coefficients used in the calculation were taken from Hill [12]. Abel inversion was performed to obtain the radial profiles of the plasma temperature and the electron number density.

3. Mathematical model

The plasma is considered axisymmetrical and in local thermodynamical equilibrium. The two-dimensional, time-dependent governing equations consist of the conservation of mass, energy, momentum, electromagnetic field, as well as those of the turbulent kinetic energy and the dissipation rate of the turbulent kinetic energy, which are based on the renormalization group (RNG) *k-e* turbulence model. The model equations are written into a general form:

$$\frac{\partial}{\partial t}(rf)+\frac{\partial}{\partial z}(ruf)+\frac{1}{r}\frac{\partial}{\partial r}(rrvf)=\frac{\partial}{\partial z}\left(\Gamma_f\frac{\partial f}{\partial z}\right)+\frac{1}{r}\frac{\partial}{\partial r}\left(r\Gamma_f\frac{\partial f}{\partial r}\right)+S_f\,. \tag{1}$$

Table I. Variables, coefficients and source terms for the conservation equations.

f	Γ_ϕ	S_ϕ
1	0	0
u	m_e	$-\frac{\partial p}{\partial z}+\frac{\partial}{\partial z}\left(m_e\frac{\partial u}{\partial z}\right)+\frac{1}{r}\frac{\partial}{\partial r}\left(rm_e\frac{\partial v}{\partial z}\right)+F_z$
v	m_e	$-\frac{\partial p}{\partial z}+\frac{\partial}{\partial z}\left(m_e\frac{\partial u}{\partial r}\right)+\frac{1}{r}\frac{\partial}{\partial r}\left(rm_e\frac{\partial v}{\partial r}\right)-\frac{2m_e v}{r^2}+\frac{rw^2}{r}+F_r$
w	m_e	$-\frac{w}{r}\left(rv+\frac{m_e}{r}+\frac{\partial m_e}{\partial r}\right)$
h	$k/C_p+m_t/\mathrm{Pr}_t$	P_0-P_R
k	$a_k m_e$	$G-re$ *
e	$a_e m_e$	$\frac{e}{k}(C_{e1}G-C_{e2}re)-R$ **

* $G=m_t\left\{2\left[\left(\frac{\partial u}{\partial z}\right)^2+\left(\frac{\partial v}{\partial r}\right)^2+\left(\frac{v}{r}\right)^2\right]+\left(\frac{\partial w}{\partial r}-\frac{w}{r}\right)^2+\left(\frac{\partial w}{\partial z}\right)^2+\left(\frac{\partial v}{\partial r}+\frac{\partial u}{\partial r}\right)^2\right\}$

** $R=\frac{C_m rh^3(1-h/h_0)}{1+bh^3}\frac{e^2}{k}$

$h\equiv Sk/e$, $S^2=G/m_t$, $m_e=m_m+m_t$, $m_t=rC_m k^2/e$, $h_0=4.38$, $b=0.012$, $\mathrm{Pr}_t=0.7$, $C_m=0.0845$, $C_{e1}=1.42$, $C_{e2}=1.68$, $a_k=a_e=1.39$

Table II. Torch dimensions and operating conditions.

Inner radius of central tube (R_1)	1.0 mm	Central gas flow rate (Q_1)	0 slpm
Outer radius of central tube (R_2)	2.0 mm	Plasma gas flow rate (Q_2)	0 slpm
Radius of sheath tube (R_3)	27.0 mm	Sheath gas flow rate (Q_3)	98 slpm (Ar)
Inner radius of torch (R_0)	27.5 mm		6 slpm (H_2)
Radius of RF coil (R_c)	44.0 mm	Plasma power (P_0)	4–13 kW
Position of first RF coil (L_1)	60.0 mm	Pressure (p)	27 kPa
Position of last RF coil (L_2)	145.0 mm	Numer of RF coil (N_c)	13 turn
Length of torch (L_3)	170.0 mm	Operating frequency (f)	1 MHz
Thickness of torch wall (d_w)	7.5 mm		

The dependent variables, the transport coefficients and the source terms are summarized in Table I, and detailed descriptions of the model and the solution method are found in Ref. 11.

4. Results and discussion

Computations were performed for the PM-ICP under the operating conditions given in Table II. In Figure 2, the left-hand side depicts the predicted isotherms under the continuous power condition (13 kW), and another side presents the time-averaged ones over one pulse cycle (15 ms) under the pulsed power condition. Compared to the continuous plasma, the high temperature zone was much smaller in the pulsed power plasma, and the

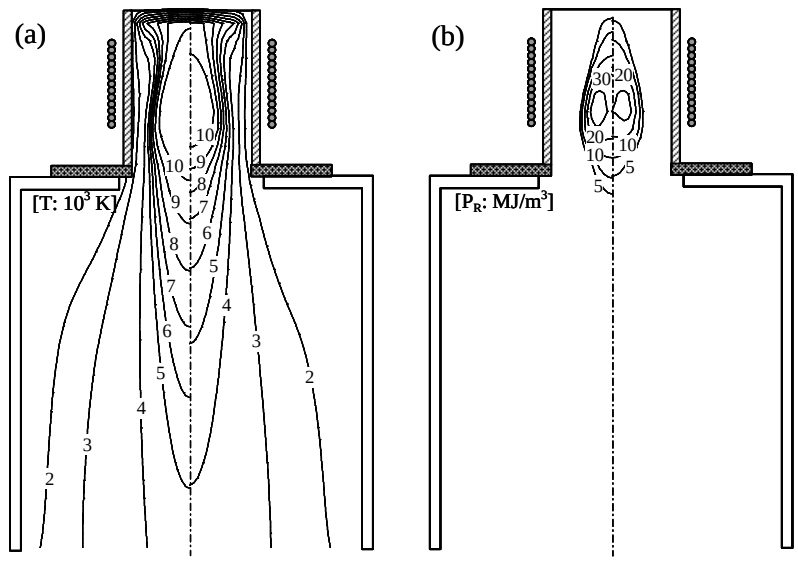

Figure 2. Predicted temperature fields (a) and volumetric radiation power (b) for the continuous plasma (left-hand side) and the pulse-modulated plasma (right-hand side).

plume length of the time-averaged plasma was also much shorter. Along the axis, in the downstream of the torch the time-averaged temperatures were 1000–1500 K lower than those of the steady-state at the same axial position. The volumetric radiation power was also reduced considerably in the pulsed power plasma. Consequently a specimen can be put closer to the discharge zone of the pulse-modulated plasma and better irradiation effects may be achieved.

Figure 3 illustrates the predicted and measured profiles of plasma temperatures at 10 mm below the end of the coil (z=155 mm). Although the measured plasma temperatures were found scattered around, most of them were about 1000–2000 K higher than the predicted ones. This phenomenon could be attributed to the fact that the measured temperatures were actually the excitation temperatures which were closer to those of the electrons, and therefore were higher than the heavy particle temperatures. In addition, under the pulsed power condition, the radial temperature gradients became less steep, and more uniform plasma temperature profiles could be obtained.

The electron number densities under given pressure and temperature conditions were calculated using a chemical reaction kinetics model [12]. In Figure 4, the predicted and measured time-averaged electron number densities were very close to each other in the central region of the torch (r<12 mm), but the differences between these two densities increased with the radial position. The measured electron number densities only had slight decreases at the boundaries of the plasma where the emission signals could be detected. However, the predicted ones dropped significantly in the fringes of the plasma. The differences between the predicted and measured results were beyond the ranges of experimental errors, and could be ascribed to the presence of nonequilibrium phenomena in these regions. Taken into account the radial diffusion of species, the electron temperatures and number densities at the boundaries under nonequilibrium conditions should be much higher than those values under equilibrium conditions owing to the high mobility of electrons [13]. Consequently, rather than using the LTE temperature, the electron number densities should be evaluated using nonequilibrium models that could include the effects of temperatures for different species. In Figures 4 and 5, we may find that the departure from LTE became more significant as the plasma flowed downward and cooled down.

Moreover, the results indicated that the deviation from equilibrium became more noticeable under the pulse-modulated operating condition. The nonequilibrium regions even extended into the central region where the plasma was normally in equilibrium under the continuous operating condition, see Figure 5. For example, at

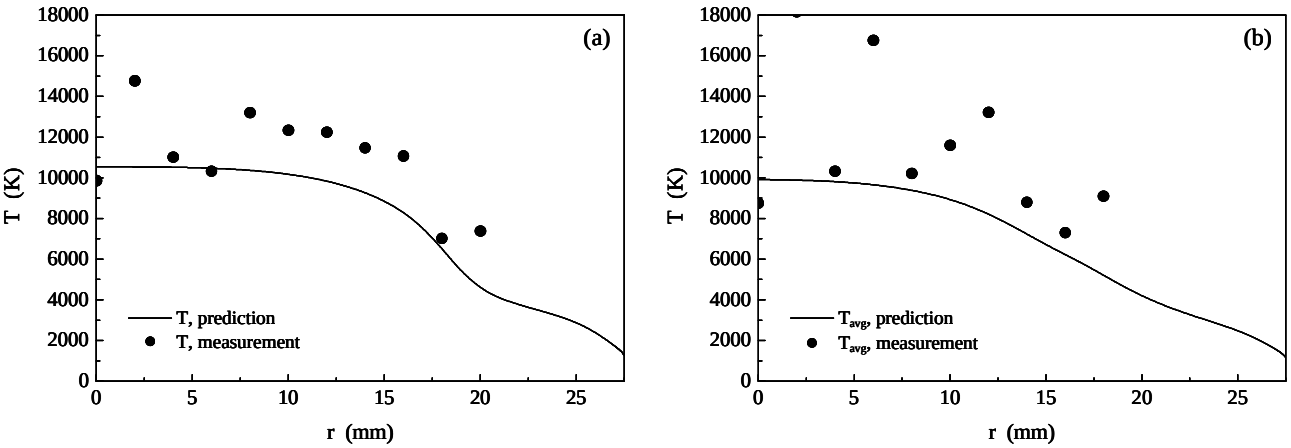

Figure 3. Predicted and measured temperatures at 10 mm below the end of the coil (z=155 mm): (a) steady-state, and (b) time-averaged.

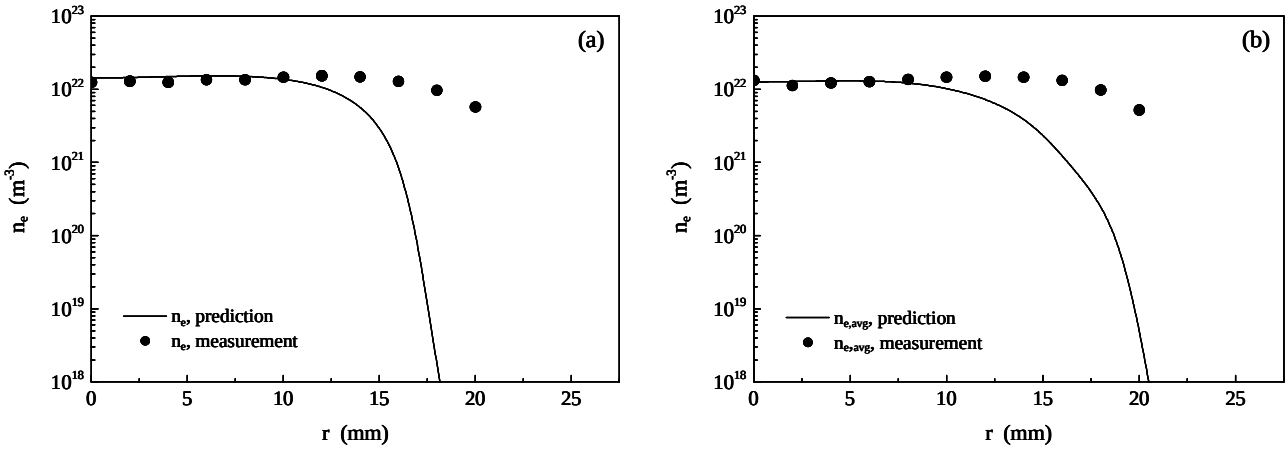

Figure 4. Predicted and measured electron number density at the midcoil (z=102.5 mm): (a) steady-state, and (b) time-averaged.

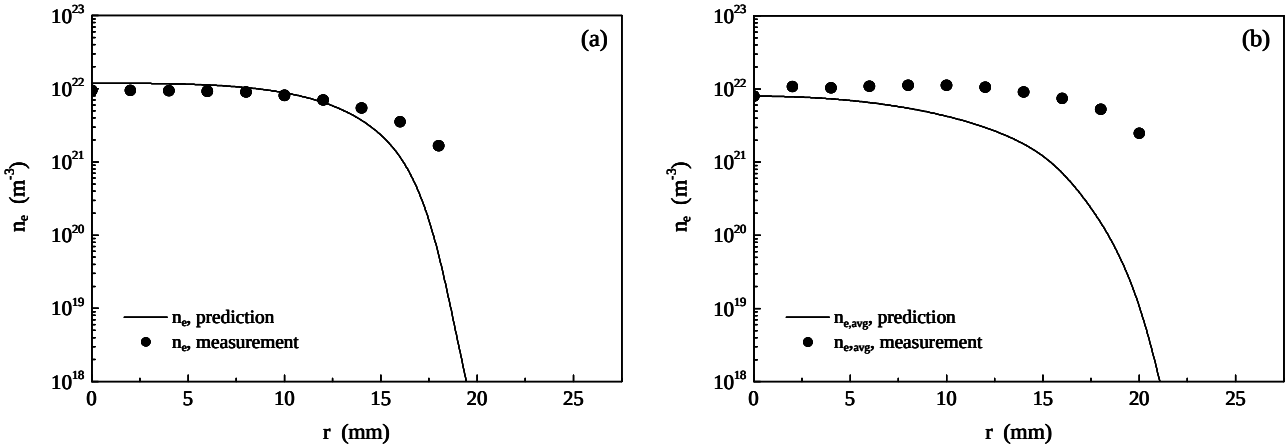

Figure 5. Predicted and measured electron number density at 10 mm below end of the coil (z=155 mm): (a) steady-state, and (b) time-averaged.

r=10 mm, the measured and predicted electron number densities were respectively 1.1×10^{22} and 4.1×10^{21} m^{-3}, the former was 2.7 times as high as the latter. This difference was due to the fact that the electrons reacted to the changes in the input power much faster than the heavy particles did, the electron temperature had a quick increase at the stage of pulse-on, and the degree of departure from LTE was enhanced under the pulsed power condition. However, the effect of electron temperature on the plasma properties was not considered in the LTE model, and the plasma composition was estimated based on the equilibrium temperature. As a result, the electron number densities might be underestimated when the plasma deviated from equilibrium.

5. Conclusion

In summary, the predicted results showed that the time-averaged temperature of the PM-ICP was much smaller than that of the continuous plasma. The measured plasma temperatures had similar radial profiles to the predicted ones, although the former were a bit higher. The agreement between the theoretical and experimental electron number densities was satisfactory in the central region of the torch, but the discrepancies became larger in the fringes of the plasma where the deviation from LTE was the most pronounced. It was suggested that the LTE model might not be accurate enough to adequately describe the behavior of plasmas under such pulsed power conditions. Our work involving the development of non-LTE models for PM-ICPs is on-going.

Acknowledgement

The Japan Society for the Promotion of Science (JSPS) is greatly acknowledged for providing a JSPS research fellowship to R. Ye.

References

[1] T. Ishigaki, X. Fan, T. Sakuta, T. Banjo, and Y. Shibuya, Appl. Phys. Lett. **71**, 3787 (1997).
[2] T. Sakuta, K. C. Paul, M. Katsuki, and T. Ishigaki, J. Appl. Phys. **85**, 1372 (1999).
[3] T. Sakuta and T. Ishigaki, Pure Appl. Chem. **71**, 1845 (1999).
[4] Y. Tanaka and T. Sakuta, Plasma Source Sci. Technol. **12**, 69 (2003).
[5] T. Ishigaki, N. Okada, N. Ohashi, H. Haneda, and T. Sakuta, Pure Appl. Chem. **74**, 435 (2002).
[6] N. Ohashi, T. Ishigaki, N. Okada, T. Sekiguchi, I. Sakaguchi, and H. Haneda, Appl. Phys. Lett. **80**, 2869 (2002).
[7] N. Ohashi, T. Ishigaki, N. Okada, H. Taguchi, I. Sakaguchi, S. Hishita, T. Sekiguchi, and H. Haneda, J. Appl. Phys. **93**, 6386 (2003).
[8] J. Mostaghimi, K. C. Paul, and T. Sakuta, J. Appl. Phys. **83**, 1898 (1998).
[9] M. M. Hossain, Y. Hashimoto, Y. Tanaka, K. C. Paul, and T. Sakuta, IEEE Trans. Plasma Sci. **30**, 327 (2002).
[10] K. C. Paul, T. Ishigaki, J. Mostaghimi, and T. Sakuta, J. Appl. Phys. **93**, 8867 (2003).
[11] R. Ye, T. Ishigaki, and M. I. Boulos, J. Appl. Phys. **96**, 118 (2004).
[12] E. Richley and D. T. Tuma, J. Appl. Phys. **53**, 8537 (1982).
[13] J. Mostaghimi, P. Proulx, and M. I. Boulos, J. Appl. Phys. **61**, 1753 (1987).